Three-dimensional voltammetry: use of chronoamperometric E-t-i data to achieve second-order advantage

Sherlan Guimarães Lemos [a]*, *Jose González-Rodríguez* [b]

[a] Department of Chemistry, Federal University of Paraíba, 58051-970, João Pessoa, PB, Brazil

[b] School of Chemistry, College of Science, University of Lincoln, Brayford Pool, Lincoln, LN67TS, United Kingdom

*Corresponding author: sherlan@quimica.ufpb.br (Sherlan G. Lemos)

ABSTRACT

This work studied the use of three-dimensional voltammetry, particularly potential-time-current (E-t-i) data, on the development of electroanalytical methods. E-t-i data was obtained by taking chronoamperograms at potentials applied as pulses on a staircase waveform. By using this three-way kind of data and appropriate calibration algorithms, the possibility of achieving the second-order advantage was evaluated in the determination of ferrocyanide in the presence of the uncalibrated interference hydroquinone as a model system. The determination of acetaminophen in urine samples, where ascorbic acid and uric acid play the major roles as interferents was also studied. Parallel factor analysis (PARAFAC) and multivariate curve resolution alternating least-squares (MCR-ALS) were the algorithms employed in this work. Both algorithms successfully achieved the second-order advantage by correctly predicting the concentrations of the validation synthetic samples. Excellent predictions were obtained in the direct analysis of acetaminophen-spiked urine samples by E-t-i data and MCR-ALS.

Keywords: Chronoamperometry; Three-Dimensional Voltammetry; Chemometrics; Multivariate Calibration; Paracetamol; Urine

1. INTRODUCTION

The first mention to the use of a three-dimensional representation of electrometric properties was made by Reilley et al. in 1951 [1], with a unified model based on a three-dimensional surface comprising current, voltage, and percentage of a substance in the oxidized state. Following this, Reinmuth [2] introduced the use of three-dimensional surfaces based on potential-time-current relationships in 1960. Developed under theoretical basis, both papers aimed at showing and explaining the relationships established among various time-independent and time-dependent electrometric techniques such as polarography, voltammetry, chronoamperometry, and chronopotentiometry. The visionary aspect of the work developed by both authors was important to the development of the first practical application on three-dimensional electrochemistry by Anderson and Bond [3] in 1983. The authors by that time were aware of the valuable potential of three-dimensional techniques in other areas of chemistry and expected the same for electroanalytical chemistry. The experimental difficulties to implement three-dimensional electrochemistry were only overcome thanks to the availability of adequate computerized instrumentation in the beginning of the 1980's. They obtained normal pulse polarographic data from several time domains in a single experiment, representing data as potential-time-current (E-t-i) surfaces. They verified that this approach was more efficient on detecting different types of interferences than one time-domain electrochemical data only, given the higher sensitivity of variable time domain electrochemical data regarding different kinetic phenomena.

E-t-i surfaces have usually been based on double potential step chronoamperometric data, where the initial potential was always at that point where no faradaic processes occurred and stepped up using incremental potentials and recording the current-time curves. Consequently, the first applications of three-dimensional electrochemistry, or also three-dimensional voltammetry [4],

were mainly based on the elucidation of the kinetics and mechanisms of electrodic reactions [4,5,6,7] and formation of complexes [8]. Chronoamperometry is a very favourable technique for this aim because of its high sensitivity when plotted as a function of potential. All the available information from the electrodic processes is embodied in the three-dimensional E-t-i surface [7]. Analytical applications can also be found regarding the early stages of three-dimensional electrochemistry [3,9]. They were based on the collection of univariate information such as peak height, peak position, and peak width at half-height at a range of pulse times, which were used to diagnose interference effects and indicate whether direct calibration or standard addition should be applied.

As the E-t-i surfaces encompass the use of more than one time-domain in the same electrochemical experiment, they can be classified as second-order data, or three-way data. In this kind of data, multivariate signals are collected per sample and organized into a data table or matrix in a way that the sample's analytical signal is characterized by having more than one mode or domain. For example, in the case of E-t-i data the *t-i* mode contains a collection of chronoamperograms at several *E* values, while the *E-i* mode contains a set of voltammograms over a given time period. By combining second-order electrochemical data with suitable calibration methodologies, such as parallel factor analysis (PARAFAC) [10] or multivariate curve resolution by alternating least squares (MCR-ALS) [11], the second-order advantage [12] can be achieved , which allows the quantification of the analyte in the presence of unknown interferents.

This remarkable feature is possible because, once adequately decomposed by a suitable algorithm, the information provided by second-order data can be uniquely ascribed to the analyte, even in the presence of components not considered at the calibration stage. In consequence, the second-order advantage allows the construction of calibration models obtained from simpler

standards that can be used directly on complex samples. An additional advantageous feature of some second-order calibration methods is that they operate by converting the analytical signal into the profiles of the pure components, which also allows for the qualitative characterization of the analytes. Thus, as one can conclude, the first analytical applications of three-dimensional voltammetry did not seize the full potential of the E-t-i surfaces.

The first work describing the association between second-order electrochemical data and multivariate calibration techniques in order to achieve the second-order advantage was presented by Galeano-Díaz et al. [13] for the simultaneous determination of fenitrothion, fenitrooxon and 3-methyl-4-nitrophenol in environmental samples in 2008. To obtain the three-way data, they used square wave voltammograms taken at different accumulation times as the second-order domain. Since then, although still incipient, the number of applications involving second-order multivariate calibration of electrochemical data has increased. It has become the most employed strategy to drive second-order electrochemical data the in-series execution of voltammograms by changing one of the instrumental parameters. These would be either the pulse time [14] or pulse amplitude [15,16,17] in differential pulse voltammetry or the frequency in square wave voltammetry [18,19].

It is remarkable that, although it was the preferred approach in the first decades of three-dimensional voltammetry, E-t-i data obtained from chronoamperometric measurements had not been used to develop analytical applications based on the second-order advantage. This was the case despite the alleged higher sensitivity to small changes in electrochemical behavior and higher amount of electrochemical information presented by such type of data [3,20]. It is well known that the resolution between two overlapping voltammetric processes depends largely upon the half-wave potential ($E_{1/2}$) values, the concentration ratios and the kinetics of the electron transfer [21]. Thus, for example, if two overlapping processes are kinetically different in the context of the

electron transfer being the rate determining step, then the multi-time-domain electrochemical measurements could provide a useful way of discriminating against one of the processes, as long as measurements were made at longer time domains [22].

The work presented here aimed at the evaluation of E-t-i data in association with second-order calibration techniques in the development of electroanalytical methods. The methodology was initially evaluated with a model problem, namely the determination of ferrocyanide – a well-known redox probe with well-reported electrochemical behavior [23,24] – in the presence of hydroquinone, as a strong interferent not included in the calibration step. Ferrocyanide and hydroquinone show highly overlapped voltammetric peaks, but distinct oxidation processes regarding electron transfer. Following, the same method was applied in the direct determination of acetaminophen in urine samples, in the presence uric acid, ascorbic acid, and 3-acetamidophenol as uncalibrated interferents.

Acetaminophen (4-acetamidophenol), also known as paracetamol, is a very popular analgesic and antipyretic drug contained in many prescription and over-the-counter products [25]. The ubiquitous excretion of acetaminophen in urine has been related to exposure to aniline (or aniline-releasing substances) as well as nutrition, alongside the direct use of acetaminophen as a drug [26]. In the voltammetric determination of acetaminophen in body fluids, the presence of concomitants such as uric acid (the primary product of purine metabolism) and ascorbic acid (widely found in association with various pharmacologically active substances including acetaminophen [27]) are considered a significant issue in the accuracy of the results because the oxidation peaks are overlapping on traditional electrodes. With regard to 3-acetamidophenol, it was included as an interferent due to its chemical similarity with acetaminophen – it is a non-hepatotoxic regioisomer of acetaminophen with analgesic properties [28].

In both studies, E-t-i data were obtained by measuring the current during a series of pulses applied on a staircase waveform and the possibility of exploiting the second-order advantage was investigated by employing well-stablished algorithms, PARAFAC and MCR-ALS. PARAFAC is an algorithm used in second-order calibration that requires the data to follow a trilinear model [10]. If trilinearity is lost in one mode, then MCR can be applied, where the second-order data is unfolded in a matrix in the direction in which the loss of trilinearity occurs [11]. Thus, the MCR algorithm decomposes the data matrix in a bilinear model by alternating least squares (ALS).

2. EXPERIMENTAL

2.1. Reagents and materials

The following reagents were used: potassium dihydrogen phosphate, sodium hydroxide, potassium ferrocyanide, potassium chloride, hydroquinone, acetaminophen, uric acid, ascorbic acid, and 3-acetamidophenol. All chemicals were of analytical grade, used without further purification, and purchased from Sigma–Aldrich, except for potassium dihydrogen phosphate, which was purchased from Fisher Scientific. Ultrapure water (resistivity ≥18 MΩ·cm), produced by an ELGA purification system, was used throughout the experiments. Morning midstream human urine samples were collected from a volunteer in polystyrene urine collection bottles and were directly used to avoid degradation.

2.2. Electrochemical procedure

Electrochemical measurements were performed in a potentiostat Autolab PGSTAT302N (Metrohm Autolab, The Netherlands) controlled by software Nova 2.1 in a conventional three-

electrode electrochemical cell. The reference and auxiliary electrodes were an Ag/AgCl (3M KCl) electrode and a platinum sheet electrode, respectively, both purchased from Metrohm, UK (Part Numbers 6.0733.100 and PT.SHEET, respectively). Two working electrodes were used: i) a platinum rod electrode (Metrohm, UK, Part Number 6.0343.000); ii) carbon screen-printed electrodes obtained from Dropsens, Spain (Ref. 110). All measurements were carried out at room temperature (21±1°C) in a 50 mL cell with a quiescent pH 7.2 phosphate buffer solution used as supporting electrolyte without convection. This solution was 0.1 mol L^{-1} KH_2PO_4 + 0.1 mol L^{-1} KCl adjusted to the desired pH with NaOH 2 mol L^{-1}.

E-t-i data was obtained by performing chronoamperograms at potentials applied as pulses on a staircase waveform. Starting potential was 0.0 V, where only background current was observed in the cyclic voltammograms of ferrocyanide or acetaminophen and continued with 0.02 V increments up to 0.50V in the determination of ferrocyanide, and up to 0.80V in the determination of acetaminophen. For ferrocyanide, chronoamperograms were recorded during 10 s with sampling time of 0.5 s, and for acetaminophen, chronoamperograms were recorded during 5 s with sampling time of 0.2 s. This protocol resulted in data matrices sizes of 20 x 27 and 25 x 41 for each experiment for ferrocyanide and acetaminophen determinations, respectively.

2.3. Case studies

The study was conducted throughout two stages. The first stage aimed at evaluating the E-t-i data in the determination of ferrocyanide with second-order multivariate calibration algorithms in two different concentration ranges, 0.02-0.10 mmol L^{-1} and 0.10-1.00 mmol L^{-1}. The ability of E-t-i data in achieving the second-order advantage was evaluated by predicting ferrocyanide in the presence of hydroquinone as the unexpected sample constituent with a strong interference

behavior. Only ferrocyanide was considered to be present in the calibration samples, whereas hydroquinone was included in the validation samples. Thus, aqueous standards containing ferrocyanide in three levels – 0.2, 0.5, and 0.8 mmol L^{-1} – were prepared and hydroquinone concentration was changed from ten times lower to ten times higher the ferrocyanide concentration at each level (Table 1). Measurements at this stage were performed with a platinum rod electrode and carried-out in triplicate.

In the second stage of this work, second-order multivariate calibration with E-t-i data was evaluated in the determination of acetaminophen directly in urine samples. First, platinum rod and carbon screen-printed electrodes were tested for the determination of acetaminophen in aqueous standard solutions in the 20-100 μmol L^{-1} concentration range. A better analytical performance was obtained by using screen-printed electrodes. Consequently, they were applied in the determination of acetaminophen in the presence of the uncalibrated urine sample concomitants uric acid and ascorbic acid, which also present strong interference in its voltammetric determination, and 3-acetamidophenol, a regioisomer of acetaminophen. The experiments were carried-out following a four three-level factors orthogonal array design (Table 2) [29].

2.4. Data analysis: algorithms and procedures

PARAFAC requires the three-way data array to follow a trilinear model:

$$\underline{X} = A(C|\otimes|B)' + E \quad (1)$$

where $\underline{X}$ is the trilinear data array, A is the intensity matrix (scores matrix, sample mode), B and C are loadings matrices with the profiles of the pure components in both dimensions (*i-t* and *E-i* modes, respectively), and E is a matrix with the residues left by the model. B and C matrices are normalized. The symbol $|\otimes|$ is the operator of the Khatri-Rao product [30]. From a set of standards,

one can construct a pseudounivariate calibration curve that relates the A scores of PARAFAC to the concentrations. A three-dimensional array will be trilinear provided the following conditions are fulfilled: (i) the maximum signal measured for a pure component in each data dimension is directly proportional to the component concentration; (ii) the signal for a given sample is bilinear, i.e., data matrix can be decomposed into the product of two vectors, each containing the component profile in one of the two data dimensions; (iii) the shape of the profile for a given component in a dimension must be the same in different samples, with intensity variations being only due to different concentrations [31].

In E-t-i data, the maximum current in the E-i dimension (peak current of the voltammogram) is proportional to the concentration of the pure component. On the other hand, the maximum current in the dimension t-i (chronoamperograms) occurs at t = 0 s, where the charge current has a much greater contribution than the faradaic current; consequently, the total current is not proportional to the analyte concentration. However, as the charge current decays exponentially and long time-steps were used (0.5 s), at any t > 0 the current will have a greater contribution from the faradaic component and will be proportional to the analyte concentration. Consequently, to meet condition (i), the first point in the chronoamperograms was discarded. The fulfillment of conditions (ii) and (iii) will depend on the occurrence of phenomena that introduce non-linearity to the signals such as baseline drift and peak shift.

Peak shift in an electrochemical measurement may be due to the degradation of the reference electrode over time [32], the kinetics of heterogeneous reactions taking place at the surface of electrode, and the relation between such kinetics and the concentration of compounds in the bulk [33,34]. Once peak shift hinders the direct application of second-order data processing algorithms, the alignment of all voltammograms to the same reference position is an important

stage which should be conducted before PARAFAC. In this work, the correlation optimized warping (COW) algorithm was used to align the signals. COW alignment parameters were obtained after carrying out an automatic selection routine [35] on calibration data set. This routine automatically optimizes the segment length and slack size for COW alignment pre-processing and is available in the package created by Skov et al. [35]. The default reference vector – maximum cumulative product of correlation coefficients – was used in the optimization process.

The verification of trilinearity in PARAFAC was done through the core consistency diagnostic (CORCONDIA) [36]. It was also used in conjunction with residual fit analysis to select the correct number of components in PARAFAC models. Direct trilinear decomposition (DTLD) was used for initialization of PARAFAC decomposition of the three-way data. Usually, trilinear systems do not require any special restrictions for PARAFAC processing. But, in some occasions, the use of some constraints – orthogonality, non-negativity or unimodality – may be necessary for the resolution of the pure component profiles or to improve the interpretability or the accuracy of the model. In this case, non-negativity in mode A (scores matrix) was used.

Of the several approaches that use PARAFAC as the basis for calibration [37], one of the two most used was performed [38], which was also adopted for MCR-ALS: the I x J x K array of I calibration samples is augmented with the sample data to be predicted to form an array of dimensions (I+1) x J x K, and PARAFAC simultaneously models both the calibration and the test sample [38]. This procedure is best suited to achieve the second-order advantage, since each test sample can have its own interferents, and the sample model is best adjusted to its composition, although the construction of a single model for more than one test sample can be feasible when test samples have similar qualitative, but different quantitative composition [39]. All predictions

shown for validation and real samples throughout this manuscript were obtained by using this same procedure.

As one of the most used second-order calibration algorithms, MCR-ALS was also evaluated in the analysis of E-t-i data. MCR-ALS is an algorithm capable of handling data sets deviating from trilinearity. MCR-ALS was performed on a column-wise augmented data matrix. The data matrices obtained for the standards of the calibration set plus one test sample were put over each other in a column-wise manner, resulting in the augmented matrix D_{aug}. In E-t-i data is expected that profile variations could occur matrix-to-matrix along the E-i (voltammetric) direction caused by peak shifts and peak shape changes, producing a decrease in linearity. Thus, the strategy of augmenting matrices along the mode that is suspected of breaking the trilinear structure was carried out.

The bilinear decomposition is performed on the created column-wise augmented matrix D_{aug} according to the expression:

$$D_{aug} = C_{aug} S^T + E_{aug} \quad (2)$$

in which the rows of D_{aug} contain the voltammograms as a function of time, the columns of C_{aug} contain the chronoamperometric profiles of the resolved compounds involved in each experiment (standards and sample), the columns of S contain their related voltammograms, and E_{aug} is an augmented matrix of residuals. In this case, the resolved pure voltammograms are common to all experiments and the chronoamperometric profiles can be different from experiment to experiment, i.e., they can be concentration dependent. Thus, the areas under the chronoamperometric profiles were used to build a calibration curve.

Decomposition of D_{aug} is achieved by alternating least-squares under suitable constraints, which also help the algorithm to provide solutions with physical meaning. The applied constraints were unimodality in the voltammetric profiles, non-negativity in the chronoamperometric profiles,

correspondence among species and samples, and correlation. Before decomposition, D_{aug} was submitted to a peak shift correction procedure by performing the COW algorithm in the same way as described for PARAFAC.

MCR-ALS needs initialization with the number of components or electrochemical processes contributing linearly to the current as close as possible to the final results, which was obtained from singular value decomposition analysis of the D_{aug} matrix. Following, simple-to-use interactive self-modeling mixture analysis [40] was used to find an initial estimate of pure non-augmented profiles (voltammograms) of the components with 10% of noise allowed.

All data analysis was carried out within a Matlab® 9.3.0 (The MathWorks™, Inc.) environment using the toolbox MVC2 developed by Olivieri and co-workers [41], which enables second-order multivariate calibration including MCR-ALS and PARAFAC. Leave-one-out cross-validation was carried out to perform a first evaluation of the algorithms, based on the root mean-squared error of cross-validation (RMSECV) and prediction (RMSEP), and the relative error percentage (REP) [42]. It is important to mention that the cross-validation procedure adopted was performed with two purposes: i) to verify the concentration range or the working electrode best suited to the development of the calibration model; ii) to present and discuss qualitatively the decomposition results (pure chronoamperometric and voltammetric profiles) for the first time.

3. RESULTS AND DISCUSSION

3.1. Determination of ferrocyanide

The first stage of this work was to evaluate the applicability of E-t-i data in obtaining second-order calibration models. In this sense, the determination of potassium ferrocyanide was chosen as model system. This probe shows a quasi-reversible behavior and has well-established mechanism of

oxidation [43]. Also, $Fe(CN)_6^{3-/4-}$ is known as an inner sphere redox system that is sensitive to the surface structure of the electrode [44]. The cyclic voltammogram of ferrocyanide using a platinum rod electrode (Fig. S1) showed a ΔE_p = 131 mV, which could indicate the quasi-reversible behavior. The chronoamperograms of the supporting electrolyte (0.1 mol L^{-1} KH_2PO_4 + 0.1 mol L^{-1} KCl at pH 7.2) and 1.0 mmol L^{-1} $K_4[Fe(CN)_6]$ in the background solution, from 0.0 V up to 0.50 V, at the platinum rod electrode are presented as E-t-i surfaces in Fig. 1a and Fig. 1b, respectively, and as two-dimensional representations in Fig. S2a and Fig. S2b, respectively.

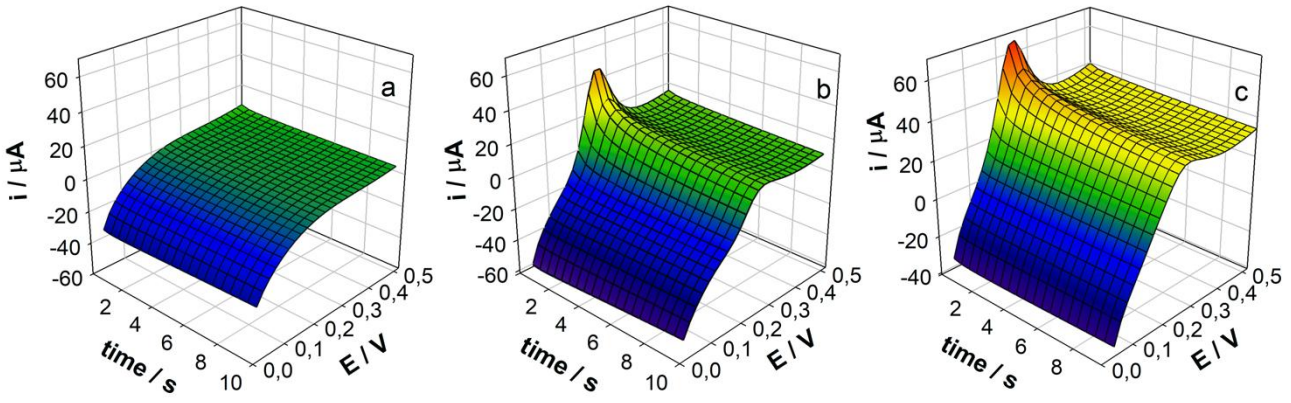

Fig. 1. E-t-i surfaces obtained at platinum rod electrode for a) supporting electrolyte, b) 1 mmol L^{-1} $Fe(CN)_6^{4-}$, and c) 0.8 mmol L^{-1} $Fe(CN)_6^{4-}$ + 0.8 mmol L^{-1} hydroquinone.

The chronoamperograms obtained for the supporting electrolyte at platinum electrode present two distinct behaviors of the current vs. time variation along the potential sweep (Fig. S2a). In the first chronoamperograms the current increases with time until it reaches a maximum value. These profiles occur with lower frequency, but with a much greater change in current over time. This behavior could be related to the dissolution the platinum working electrode in the presence of chloride ions [45,46]. As the applied potential increases, the chronoamperograms show a profile in which the current peak is obtained at t = 0 and decreases with time under a transient behavior,

similar to that of an ideal polarizable electrode. For the supporting electrolyte the currents are entirely negative during the chronoamperometric measurements at potentials lower than 0.26 V and become completely positive at potentials above 0.30 V (Fig. S2a). For ferrocyanide (Fig. 1b, Fig. S2b), at the beginning of the scan, the chronoamperograms show similar behavior to that of the supporting electrolyte. However, it changes significantly to the second behavior as it approaches the oxidation potential of ferrocyanide at 0.28 V, where a chronoamperogram with the highest currents is obtained. After this potential, similar profiles with lower currents are observed. Still, the currents are higher than those observed for the chronoamperograms of the background solution in the same region. The differences between the maximum current at t = 0 and the currents observed over time are much smaller in the chronoamperograms of the supporting electrolyte than those in the chronoamperograms of ferrocyanide.

The current measured at each point of the E-t-i surface is composed of faradaic and non-faradaic currents. The latter decays exponentially with time, while the former decays in accordance with the squared root of time for diffusive control over the rate of electrolysis [21]. The chronoamperograms of supporting electrolyte depart from the $t^{-1/2}$ dependence, which could be expected since faradaic currents are not supposed to contribute significantly to the currents registered. For ferrocyanide, chronoamperograms also deviate from the $t^{-1/2}$ dependence, except those obtained at the oxidation peak potential of 0.28 V, in accordance with the literature [21].

Initially, the calibration data sets obtained at two different ferrocyanide concentration ranges were analyzed. The first calibration set comprised five standard solutions with concentrations ranging from 0.02 mmol L^{-1} to 0.10 mmol L^{-1} $Fe(CN)_6^{4-}$. For the second calibration set, ten standard solutions were prepared in concentrations ranging from 0.10 mmol L^{-1} to 1.00 mmol L^{-1} $Fe(CN)_6^{4-}$. Briefly, for each solution, the experimentally measured chronoamperograms at

each step potential were arranged in a data matrix having as many rows as time steps and as many columns as potentials scanned during the measurements. So, each row can be considered as a voltammogram at a specified time and each column is a chronoamperogram at an applied potential.

With the calibration sets obtained, the first algorithm evaluated in order to obtain the second-order calibration models was PARAFAC. The two-way matrices obtained from the three-dimensional voltammetry experiments were arranged in a three-way array (or tensor) with dimensions 20 times × 27 potentials × 3n samples, whereas 3n means n standard solutions with increasing ferrocyanide concentration analyzed in triplicate, being n = 5 or n = 10 for the first or second calibration sets, respectively. The results of the calibration sets decompositions using PARAFAC are shown in Fig. 2. Fig. 2a and Fig. 2c show the t-i profiles (chronoamperograms) of the pure components in mode B for the 0.02 to 0.10 mmol L^{-1} $Fe(CN)_6^{4-}$ and 0.10 to 1.00 mmol L^{-1} $Fe(CN)_6^{4-}$ calibration sets, respectively, and the Fig. 2b and Fig. 2d show the pure E-i components profiles (voltammograms) in mode C. Two components presented the best compromise between the residual fit analysis and the CORCONDIA, which determined a core consistency of 100%. More components resulted in a lower residual fit, but negative core consistency values. Components have been ordered according to contribution.

The voltammetric profiles of component #1 in both calibration sets (Fig. 2b and 2d) are very similar and do not present any peaks, which could be related to the voltammogram of the background solution as the major source of variation. In the same way, chronoamperometric profiles of component #1 (Fig. 2a and 2c) show the same t-i behavior, with loadings that increase rapidly towards a nearly constant value. It could be inferred that the profile of component #1 in Fig. 2a reflects the combined effect of the two temporal behaviors observed for the

chronoamperograms of the supporting electrolyte (Fig. S2a). The same occurs for component #1 in Fig. 2c, but its correct visualization is not possible because of the wider y-axis scale necessary to depict the chronoamperometric profile of component #2. The background solution information played a significant role in the decomposition of signals in the concentration range of 0.02-0.10 mmol L^{-1} ferrocyanide. For the ferrocyanide standards containing 0.02 mmol L^{-1} up to 0.06 mmol L^{-1} it was hard to distinguish the E-t-i surface obtained in the presence of ferrocyanide from that obtained in its absence, affecting the signal-to-noise ratio and impairing the sensitivity in this range. For this reason, the prediction results obtained for this range were not satisfactory, with high RMSECV and REP values – RMSECV of 0.028 mmol L^{-1} and REP of 35% – being the 0.02-0.10 mmol L^{-1} region disregarded in the development of calibration models with PARAFAC.

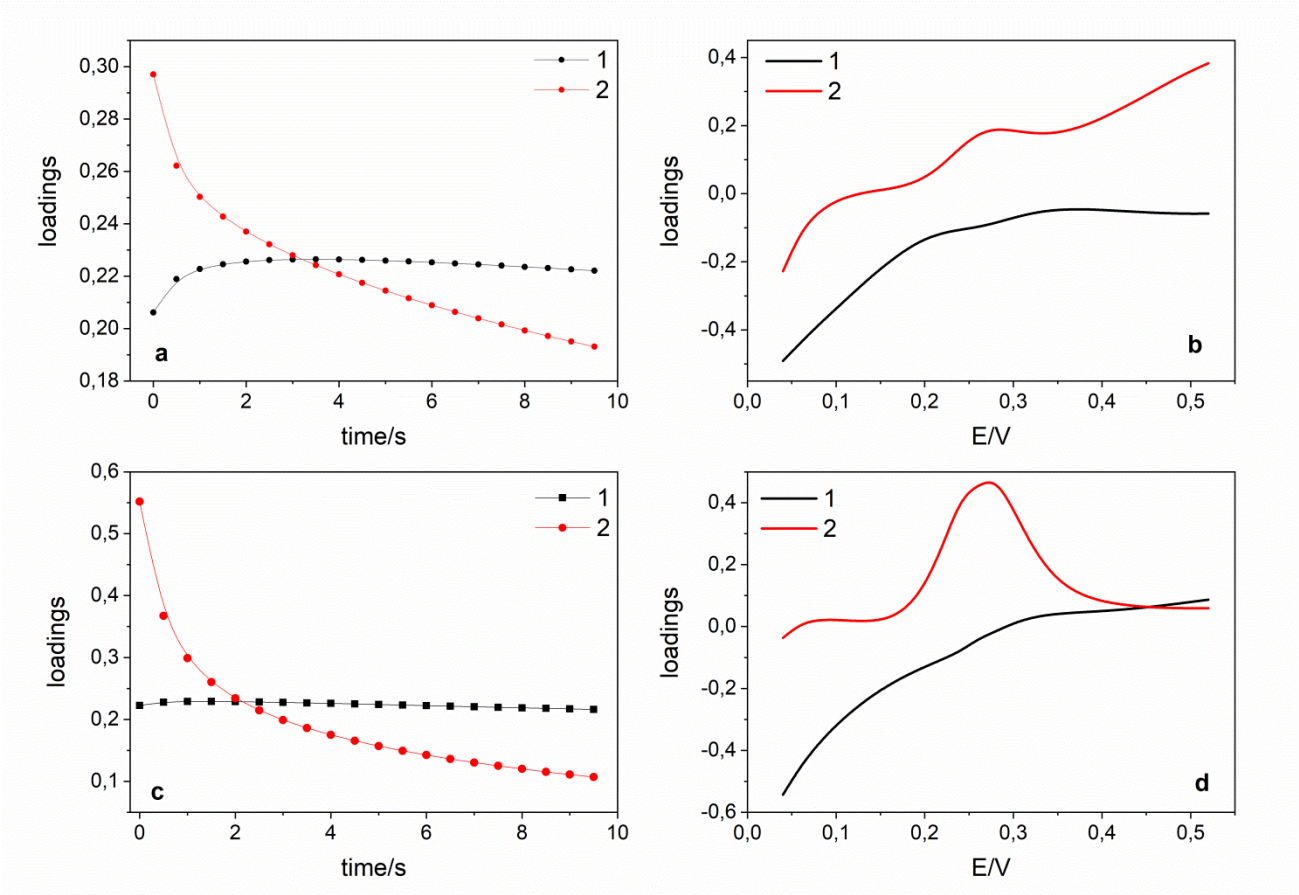

Fig. 2. PARAFAC pure component profiles obtained in B mode (a and c) and C mode (b and d) for calibration sets in the 0.02 to 0.10 mmol L^{-1} (a and b) and 0.10 to 1.00 mmol L^{-1} (c and d) ferrocyanide concentration ranges. Lines in mode B profiles do not represent a function adjusted to experimental data.

The voltammetric profiles of component #2 show a peak at about 0.28V and resemble the voltammogram of ferrocyanide (Fig. S1), the other major source of variation of the standards. Chronoamperometric profiles of component #2 reveal that at the beginning of the potential pulses, the step charging current is high and decreases with time. However, the profiles presented different exponential rates as one can verify in Fig. S3, where attempts to adjust a power function were performed. A good fit was obtained for the chronoamperometric profile of the calibration set built with higher concentrations, which presented a time decay of $t^{-0.43}$, close to that expected for a Cottrell-type decay ($t^{-0.5}$), i.e., ferrocyanide oxidation at platinum electrode is controlled by diffusion. For the calibration set with higher concentrations of ferrocyanide, PARAFAC was able to completely separate the voltammetric information of ferrocyanide from that of electrode and supporting electrolyte. One can see the near null loadings before and after oxidation peak in voltammogram #2 of Fig. 2d, contrary to what happened for voltammogram #2 of Fig. 2b, where one can recognize background information after the peak, given its strong influence on the 0.02-0.10 mmol L^{-1} range. The better resolution of the pure profiles resulted in a good prediction ability pointed by a RMSECV of 0.029 mmol L^{-1} and REP of 5% for the 0.10 mmol L^{-1} to 1.00 mmol L^{-1} concentration range.

PARAFAC was applied for the analysis of E-t-i data obtained from the validation set (Table 1). Validation set samples were produced based on the 0.10-1.00 mmol L^{-1} range and have ferrocyanide concentrations set at three levels – 0.20 mmol L^{-1}, 0.50 mmol L^{-1}, and 0.80 mmol L^{-1} –

where hydroquinone was added to reach a concentration changing from ten times lower to ten times higher the ferrocyanide concentration. Hydroquinone was chosen as an uncalibrated strong interferent due to the highly overlapped oxidation peak, as shown in Fig. S1. However, hydroquinone displays a distinctive electrochemical oxidation process in the context of electron transfer when compared to ferrocyanide [47], which can help to achieve the second-order advantage.

Table 1. Determination of ferrocyanide in the presence of hydroquinone by the application of PARAFAC and MCR-ALS. Predictions results for the validation set.

Exp.	$Fe(CN)_6^{4-}$	Hydroquinone	PARAFAC		MCR-ALS	
	Reference (mmol L^{-1})		Predicted	s.d.*	Predicted	s.d.
1-1	0.20	0.02	0.23	0.008	0.25	0.032
1-2			0.21	0.008	0.22	0.032
1-3			0.23	0.008	0.24	0.032
2-1		0.20	0.21	0.008	0.18	0.033
2-2			0.22	0.009	0.20	0.032
2-3			0.22	0.009	0.17	0.033
3-1		2.00	0.73	0.020	0.29	0.034
3-2			0.71	0.021	0.28	0.035
3-3			0.72	0.020	0.28	0.034
4-1	0.50	0.05	0.49	0.007	0.49	0.030
4-2			0.48	0.007	0.47	0.030
4-3			0.48	0.007	0.48	0.030
5-1		0.50	0.51	0.009	0.53	0.030
5-2			0.53	0.009	0.47	0.030
5-3			0.54	0.009	0.50	0.030
6-1		5.00	1.36	0.020	0.58	0.037
6-2			2.03	0.033	0.49	0.060
6-3			1.69	0.027	0.54	0.032
7-1	0.80	0.08	0.78	0.007	0.87	0.028
7-2			0.79	0.007	0.82	0.040
7-3			0.78	0.007	0.85	0.034
8-1		0.80	0.74	0.009	0.88	0.032
8-2			0.80	0.009	0.90	0.032
8-3			0.77	0.009	0.89	0.032
9-1		8.00	3.06	0.053	1.01	0.042

9-2		2.88	0.050	1.04	0.044
9-3		2.97	0.052	1.05	0.043
RMSEP (mmol L^{-1})		1.26[a] / 0.027[b]		0.10[a] / 0.050[b]	
REP (%)		250[a] / 6.1[b]		19.8[a] / 10.0[b]	

*Standard deviation (σ_y) was calculated as: $\sigma_y^2 = SEN^{-2}\sigma_x^2 + h\,SEN^{-2}\sigma_x^2 + h\,\sigma_{y_{cal}}^2$, where SEN is the sensitivity, σ_x^2 the variance in instrumental signals, *h* the sample leverage, and $\sigma_{y_{cal}}^2$ the variance in calibration concentrations. The computation of the terms comprising the equation and the details regarding other figures of merit for second-order calibration can be found in [38].

[a] Considering all validation samples

[b] Removing the validation samples with hydroquinone concentration ten times higher than the ferrocyanide concentration.

Fig. 1c shows the E-t-i data obtained from the analysis of one validation sample containing 0.80 mmol L^{-1} ferrocyanide and the same concentration of hydroquinone. One can see an E-t-i surface similar to that obtained for the sample containing 1.00 mmol L^{-1} ferrocyanide (Fig. 1b) but presenting higher currents in the chronoamperograms. Considering a sample only containing ferrocyanide at the same concentration of the experiment in Fig. 1c (0.8 mmol L^{-1}), one should expect an E-t-i surface of similar aspect, but consisting of chronoamperograms with lower currents than the surface of Fig. 1b, where the ferrocyanide concentration is higher (1 mmol L^{-1}). However, what was observed was an E-t-i surface with more intense currents at an apparently wider peak. Consequently, the interference effect produced by hydroquinone can be verified, and poor prediction results should be expected if the determination of ferrocyanide was based solely on one of the dimensions.

Table 1 shows good prediction results for PARAFAC when hydroquinone concentration is lower or at the same level of ferrocyanide concentration, providing a RMSEP of 0.027 mmol L^{-1} and a REP of 6.1%. For these samples, three components were required to give lower residual fit values. Using more components caused a decrease in the residual fit, but with negative core consistency values. Compared to the calibration set decomposition and cross-validation analysis, only one

additional component was necessary. This one is related to the presence of hydroquinone as a third source of variation. The number of components estimated was then directly related to the number of chemical components contributing significantly to the measured signals. This is possible because the experimental system behaves in a bilinear way, and no important contributions from baseline drift or other additional interference process were present.

Fig. 3a and 3b show examples of the profiles obtained in PARAFAC decomposition modes B and C for validation samples containing the same concentration of hydroquinone and ferrocyanide. One can see that the pure voltammograms and chronoamperograms of the supporting electrolyte (component 1) and ferrocyanide (component 2) were recovered in the same way as for the calibration set and in the same order of importance for decomposition. In addition, a voltammogram with a peak potential at 0.22 V is observed, which can be attributed to the presence of hydroquinone. On the other hand, the chronoamperometric profile of hydroquinone was similar to that obtained for the supporting electrolyte. It can be inferred that although the hydroquinone oxidation and the electrochemical processes related to the supporting electrolyte contribute to the total current for each chronoamperogram, its variability through the calibration and validation samples in the tensor is not sufficient to be captured in this domain, constituting two loadings profiles that have negligible variations.

Despite the good results obtained in a situation of strong interference from an uncalibrated compound, the predictions were not satisfactory when the hydroquinone concentration was tenfold higher than that of ferrocyanide (Table 1). Fig. S4 shows an E-t-i surface obtained for a sample containing 0.50 mmol L^{-1} ferrocyanide and 5.00 mmol L^{-1} hydroquinone. The surface only slightly resembles those ones from Fig.1b and Fig.1c. The higher current intensities of the chronoamperograms together with changes in the qualitative aspect of the voltammetric profiles

led to obtaining E-t-i surfaces different from those used in the calibration set. These changes produced a deleterious effect on the predictive ability of the PARAFAC.

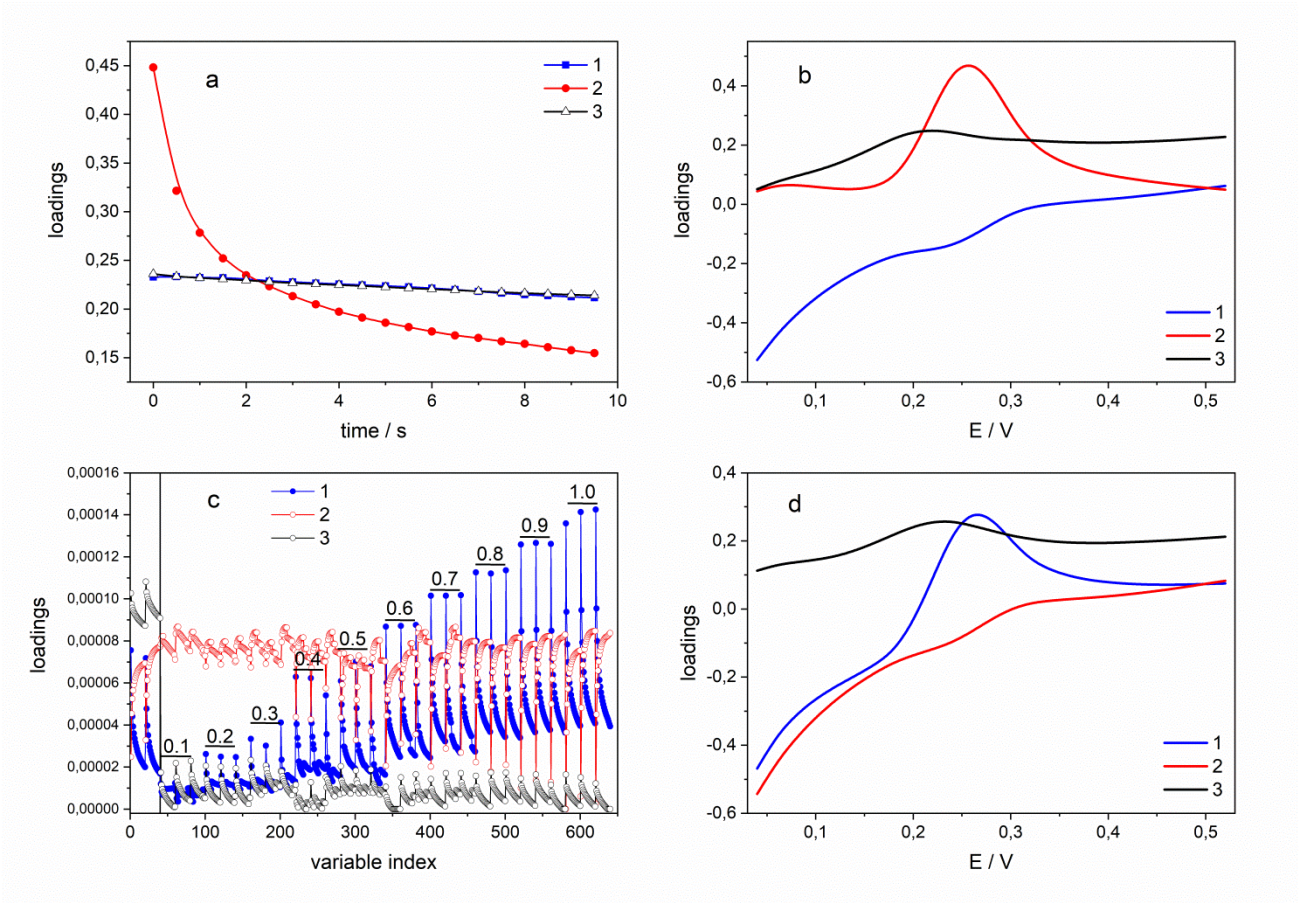

Fig. 3. Examples of PARAFAC and MCR-ALS pure component profiles obtained in B mode (a and c, respectively) and C mode (b and d, respectively) for validation samples with the same concentrations of hydroquinone and ferrocyanide. In plot c, the validation samples to the left of the vertical bar contain 0.50 mmol L^{-1} ferrocyanide and 0.50 mmol L^{-1} hydroquinone.

In order to understand how this interference occurs, Fig. S5 depicts the profiles of modes B and C obtained for the analysis of the sample on Fig. S4. The pure chronoamperograms and voltammograms of supporting electrolyte (component #2) and ferrocyanide (component #3) were properly recovered. The chronoamperogram of hydroquinone (component #1) is similar to that of

the supporting electrolyte, but its voltammogram is also similar and mirrors that of the supporting electrolyte. The lack of distinct profiles in both domains characterizes a poor decomposition of the interferent and resulted in an incorrect prediction for ferrocyanide. One can also observe that the most important component (component #1) is not related to the background solution anymore, but to hydroquinone, which indicates the severe interference of hydroquinone in this scenario. Neither the use of more components in the PARAFAC decomposition nor the use of additional constraints did resolve this issue.

The results of the decomposition of the calibration sets using MCR-ALS are shown in Fig. 4. The pure voltammograms for the calibration models obtained in the 0.02-0.10 mmol L^{-1} and 0.10-1.00 mmol L^{-1} concentration ranges are shown in Fig. 4a and Fig. 4c, respectively, and the Fig. 4b and Fig. 4d show the pure chronoamperometric profiles for each standard of the calibration set obtained in triplicate. Two components were required to provide lower values of lack of fit. As can been observed, the voltammetric profiles (Fig. 4a and 4c) of ferrocyanide (curve #1) and supporting electrolyte (curve #2) were retrieved in the same way as for PARAFAC. The chronoamperometric profiles of component #2 in Fig. 4b and 4d also show a similar t-i behavior of the loadings, increasing rapidly and following a transient behavior, which could be also related to the combined effect of the two temporal behaviors observed for the chronoamperograms of the supporting electrolyte. In addition, the corresponding chronoamperometric profiles regarding ferrocyanide seem to keep a linear relationship with the concentration of the standards. As pointed before, the areas under these chronoamperometric profiles were used to build the analytical curves. A RMSECV of 0.013 mmol L^{-1} and a REP of 22% were found for the 0.02-0.10 mmol L^{-1} range, whereas a RMSECV of 0.039 mmol L^{-1} and a REP of 7% were obtained for the 0.10-1.00 mmol L^{-1} concentration range. With MCR, as observed for PARAFAC, the supporting electrolyte information had a significant effect on the decomposition of the signals in the concentration range of 0.02-0.10 mmol

L^{-1} ferrocyanide, resulting in high RMSECV and REP values. Consequently, this range was also not considered in developing calibration models with MCR-ALS.

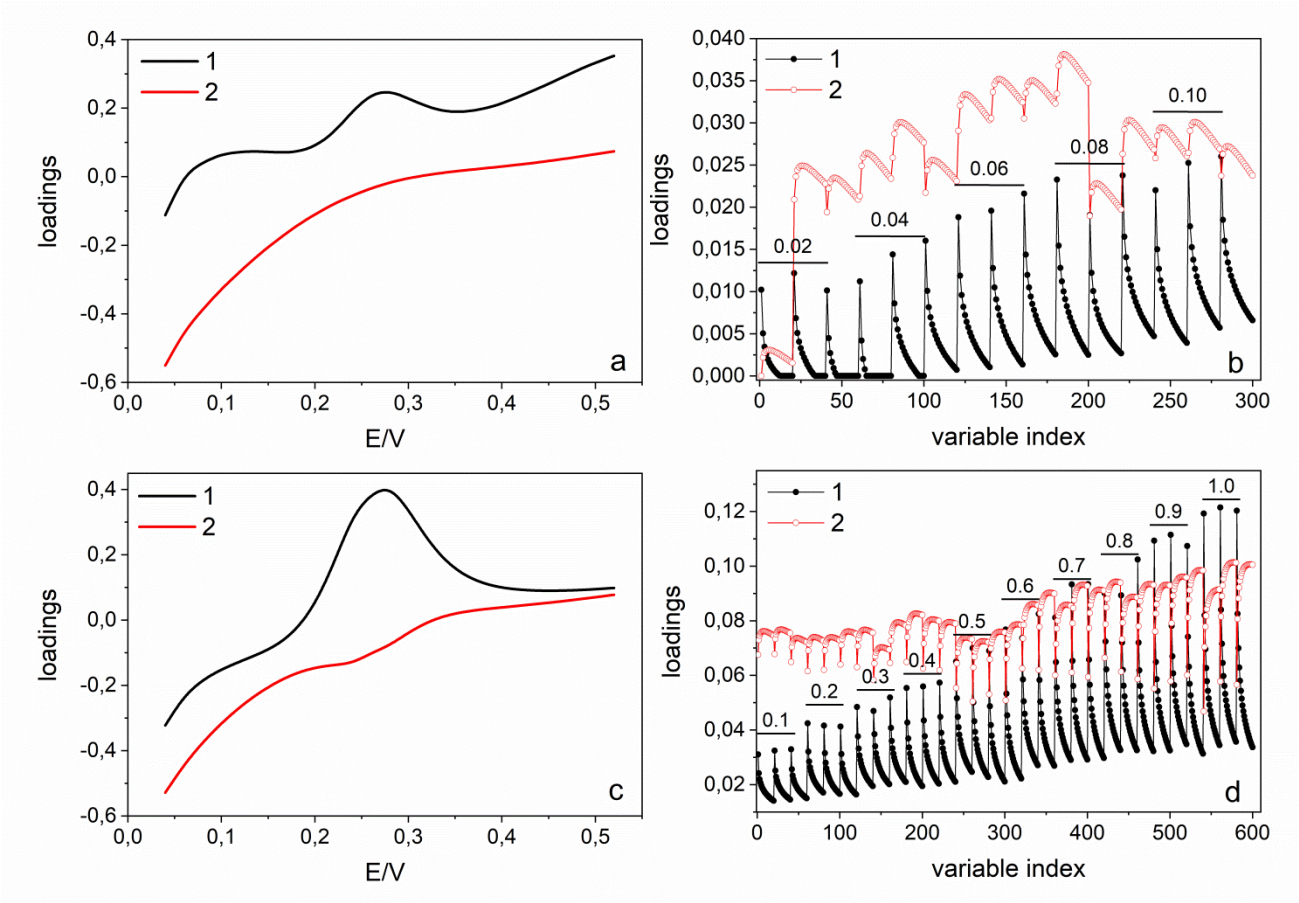

Fig. 4. Voltammetric (a and c) and chronoamperometric (b and d) profiles obtained with MCR-ALS for calibration sets in the 0.02 to 0.10 mmol L^{-1} (a and b) and 0.10 to 1.00 mmol L^{-1} (c and d) ferrocyanide concentration ranges. Lines in chronoamperometric profiles do not represent a function adjusted to experimental data.

Fig. 3c shows the chronoamperometric behavior for the analysis of two validation samples with MCR-ALS. Three components were required to achieve a successful fit. Fig. 3d shows that the pure voltammograms of ferrocyanide (curve #1) and the supporting electrolyte (curve #2) were recovered in the same way as for the calibration set. A third voltammogram with peak potential at

0.22 V was also retrieved, just like for PARAFAC, which regards to hydroquinone oxidation (curve #3). The chronoamperograms situated on the left side of the vertical line in Fig. 3c are related to the validation samples, whereas those situated on the right side are related to the calibration set standards. A set of three chronoamperograms is observed for each calibration standard. The two validation samples contain 0.50 mmol L^{-1} ferrocyanide and 0.50 mmol L^{-1} hydroquinone. One can see the good discrimination between the chronoamperograms of the analyte (component 1) and the interferent (component 3). The retrieved chronoamperograms of the interferent show higher current intensities, in agreement with the effect observed in E-t-i surfaces for this level of interference (Fig.1c). Likewise, Fig. S6 shows the chronoamperometric profiles resulting from the individual MCR-ALS decomposition of twelve validation samples containing ferrocyanide and hydroquinone. The components 1, 2 and 3 correspond to ferrocyanide, electrolyte and hydroquinone, respectively, as in Fig. 3c and 3d. It is observed that the profiles of component 3 show loadings that increase as the hydroquinone concentration increases in the samples. On the other hand, when the hydroquinone concentration is ten times lower than the ferrocyanide concentration, the profiles of component 3 have small or null loadings. These results support the assignment of component 3 to hydroquinone oxidation. The obtained chronoamperograms for the ferrocyanide component in these samples are very similar to the obtained for the correspondent standard in the calibration set.

MCR-ALS was also applied in the analysis of E-t-i data obtained from validation set (Table 1). As well as PARAFAC, MCR-ALS provided good prediction results when hydroquinone concentration was lower or at the same level of ferrocyanide concentration, with a RMSEP of 0.050 mmol L^{-1} and a REP of 10%. However, MCR-ALS also provided satisfactory predictions when hydroquinone concentration was ten times higher than ferrocyanide, except when the concentration of

hydroquinone was 8.00 mmol L^{-1}. Even so, the prediction errors in this case were much smaller than those obtained with PARAFAC.

3.2. Determination of acetaminophen

In the second stage of this work, the association between E-t-i data and PARAFAC or MCR-ALS was evaluated for the resolution of a more realistic analytical problem: the direct determination of acetaminophen in urine samples. Urine is a complex matrix that can contain several electroactive substances related to the individual's metabolism and that obviously will not be included in the calibration set. Among these substances are uric acid and ascorbic acid, which have a well-reported interfering effect on the voltammetric determination of acetaminophen [48,49]. Fig. S7 shows the cyclic voltammograms for acetaminophen, ascorbic acid, uric acid, and 3-acetamidophenol at a carbon screen-printed electrode (CSPE) and the highly overlapped oxidation peaks, which prevents the voltammetric determination of acetaminophen in the presence of these substances.

Initially, the E-t-i surface for a 100 μmol L^{-1} acetaminophen solution in the supporting electrolyte was achieved by using two distinct electrodes: Pt rod electrode (Fig. 5a) and CSPE (Fig. 5b). In Fig. 5a a similar pattern to that observed for the ferrocyanide analysis can be seen. A broad and less intense peak between 0.4V and 0.5V can be observed. On the other hand, Fig. 5b shows a sharp increase in the currents of the chronoamperograms when the potential is scanned from 0.0V up to a maximum at 0.38V, decreasing and thereafter stablishing a plateau. Hence, CSPE was chosen given its higher selectivity and sensitivity towards acetaminophen oxidation compared to Pt.

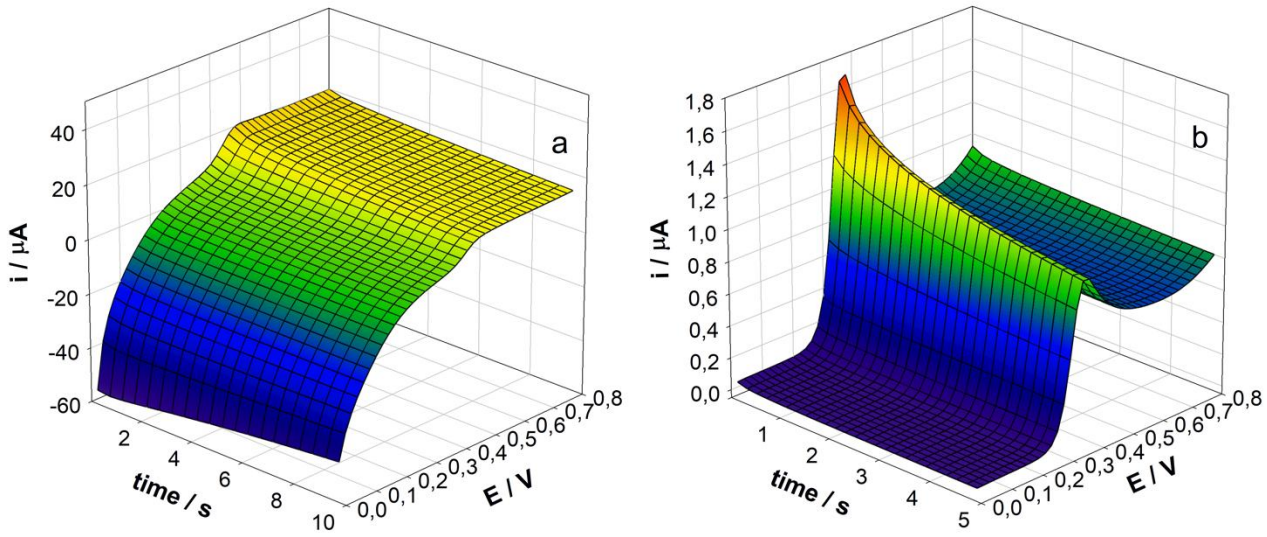

Fig. 5. E-t-i surfaces for 100 µmol L^{-1} acetaminophen at Pt (a) and CSPE (b).

E-t-i surfaces obtained for background solution and for calibration set (20-100 µmol L^{-1} acetaminophen) at carbon screen-printed electrode are depicted in Fig. S8, and the results of the decomposition of the calibration set using PARAFAC and MCR-ALS are shown in Fig. 6. Fig. 6a shows the pure voltammograms, and Fig. 6b and 6c show the chronoamperometric profiles for the calibration set retrieved by PARAFAC and MCR-ALS, respectively. Only one component was enough for both algorithms to capture data variability and to perform a successful decomposition (core consistency of 100% and low residual fit values), as the chronoamperograms of the supporting electrolyte presented very low current intensities (Fig. S8). Both voltammetric profiles in Fig. 6a show a peak at about 0.38V and resemble the positive scan of the cyclic voltammogram of acetaminophen (Fig. S7).

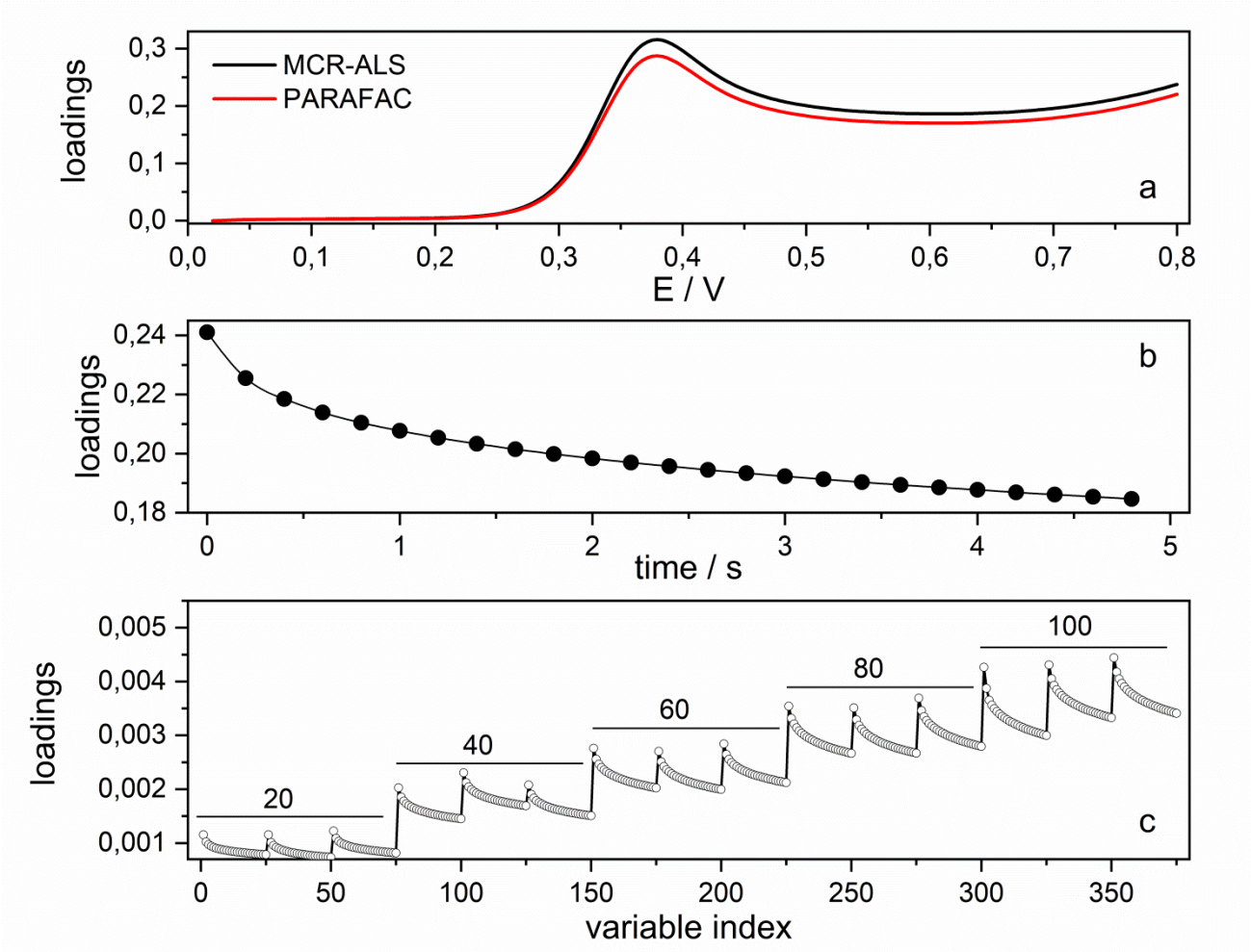

Fig. 6. Voltammetric (a) and chronoamperometric profiles obtained with PARAFAC (b) and MCR-ALS (c) for acetaminophen calibration set. Lines in chronoamperometric profiles do not represent a function adjusted to experimental data.

The pure chronoamperometric profiles shown in Fig. 6b and 6c presented a similar behavior, with a well-adjusted exponential function giving an approximate $t^{-0.1}$ decay, which departs from the Cottrell-type. Acetaminophen oxidation at neutral pH is characterized by a dimerization reaction after an electron transfer, forming a thin film of product at the surface of the electrode, inhibiting the performance of the electrode process [50]. The chronoamperometric MCR-ALS profiles in Fig. 6c keep a linear relationship with the concentration of acetaminophen, giving a good RMSECV of

5.4 mol L^{-1}. PARAFAC also provided a similar RMSECV of 5.4 μmol L^{-1}, which corresponds to a REP of 9%.

PARAFAC and MCR-ALS were both applied in the analysis of samples from a validation set containing acetaminophen and the uncalibrated interferents ascorbic acid, uric acid and 3-acetamidophenol. The samples were prepared following a four three-level factors orthogonal array design shown in Table 2. The triplicate of each experiment is given. Models required from one component when interferents concentrations were low compared to acetaminophen (experiment 1), to three components, when interferents were at concentrations at least ten times higher than acetaminophen (experiment 3). Good prediction results were observed for both algorithms.

Table 2. Prediction results of the validation set for the determination of acetaminophen (AC) in the presence of ascorbic acid (AA), uric acid (UA), and 3-acetamidophenol (MA).

Exp.	AC	UA	AA	MA	PARAFAC		MCR-ALS	
	Reference (μmol L^{-1})				Predicted (μmol L^{-1})	s.d.*	Predicted (μmol L^{-1})	s.d.
1-1	30	3	5	5	36.1	1.2	28.2	2.7
1-2					33.4	1.2	27.9	2.2
1-3					32.0	1.3	27.1	2.4
2-1		30	50	50	36.1	1.2	37.0	2.8
2-2					30.9	2.0	31.0	3.1
2-3					34.6	1.5	34.0	3.0
3-1		300	500	500	46.4	3.2	45.1	2.1
3-2					33.8	1.2	40.7	2.2
3-3					33.9	1.5	38.9	2.1
4-1	50	3	50	500	56.9	2.2	54.9	1.5
4-2					59.3	2.6	55.6	1.9
4-3					54.5	1.8	50.4	1.7
5-1		30	500	5	49.6	4.5	50.9	4.8
5-2					40.1	2.0	56.4	4.9
5-3					41.3	1.2	46.4	4.8
6-1		300	5	50	52.9	1.2	56.0	1.2
6-2					47.1	1.0	56.2	1.1

6-3					51.4	1.0	48.6	1.2
7-1					68.4	1.7	69.4	7.1
7-2		3	500	50	76.7	1.7	64.2	7.1
7-3					69.7	1.0	71.8	7.1
8-1					75.1	1.2	75.0	2.2
8-2	70	30	5	500	69.4	2.2	74.9	2.2
8-3					78.9	1.6	67.2	2.2
9-1					88.1	1.8	71.0	3.0
9-2		300	50	5	84.2	1.0	69.6	3.1
9-3					64.7	1.3	70.3	3.0
RMSEP (μmol L^{-1})					7.4		6.2	
REP (%)					15		12	

*Standard deviation calculated as informed in Table 1.

In view of the good results, E-t-i data and the second-order algorithms PARAFAC and MCR-ALS were applied to the determination of acetaminophen in real samples. Urine samples were added to a volumetric flask, spiked with different amounts of acetaminophen according to the calibration set and diluted to the mark with supporting electrolyte (1:10 dilution). Then, aliquots of the diluted samples were introduced into the electrochemical cell and the E-t-i data were recorded at CSPE. Sample data was aligned to the calibration set data with COW. For MCR-ALS, the obtained matrix was column-wise augmented to standards matrices and MCR-ALS was performed. Best predictions were obtained with MCR-ALS, which recovery rates were 89% and 100% for the spiked urine samples with concentrations of 20 μmol L^{-1} and 100 μmol L^{-1}, respectively.

PARAFAC did not present satisfactory prediction results probably due to the fact that E-t-i surfaces obtained for the urine samples have different profiles compared to those from calibration set, with chronoamperograms with very intense currents (Fig. S9). This is a situation similar to that previously observed when the concentration of hydroquinone was ten times higher than ferrocyanide. Probably, in those situations, some non-linearities are affecting more severely the data leading to a stronger violation of the trilinearity assumption. In this case, PARAFAC2 can be

performed in the specific situations in which PARAFAC did not obtain good results in order to relax trilinearity and possibly obtain better prediction results, as indicated by [38].

According to the elimination kinetics of acetaminophen, urinary acetaminophen concentration can reach maximum levels of approximately 400 mg L^{-1} between 4-12 h after intake of a single tablet of 500 mg acetaminophen and remain at about 4 mg L^{-1} (26.5 μmol L^{-1}) until 36–48 h [26]. A study comprising the analyses of 2098 spot urine samples of the general population for acetaminophen with HPLC-MS/MS found a wide range of concentrations from 0.65 μg L^{-1} to 2.27 g L^{-1}, with averages of 4.1 mg L^{-1} and 10.8 mg L^{-1} for non-smokers and smokers, respectively [26]. Additionally, urinary concentrations of acetaminophen could reach maximum levels of 10-60 mg L^{-1} during exposure to aniline – between 75-86% of an oral dose of aniline is excreted as acetaminophen [26]. The obtained calibration model is adequate for such concentration levels. Considering the mean values and the wide span of concentrations that can be found for urinary acetaminophen, the proposed method is adequate for direct acetaminophen monitoring after intake and can also be used as valid and rapid approach for acetaminophen screening.

4. CONCLUSIONS

In this study, we showed that the association between three-dimensional voltammetry based on chronoamperometric measurements and second-order calibration techniques was successful in achieving the second-order advantage in electroanalytical methods. The E-t-i data comprising chronoamperograms obtained at potentials applied on a staircase waveform were used in situations where one or more uncalibrated concomitants with a strong interfering action on the voltammetric determination of the analyte are present. PARAFAC and MCR-ALS were evaluated as calibration techniques and provided good prediction results when the interferent concentration

was lower or at the same level as the analyte. In these situations, the pure component profiles of the analyte and the interferents were properly retrieved. However, when the concentration of the interferent was ten times higher than the analyte, only MCR-ALS continued to show good prediction ability. MCR-ALS also produced better prediction results in the determination of paracetamol in urine samples. The analytical method proposed for direct analysis of urine samples for paracetamol determination is experimentally simpler, once it requires only sample dilution, and has low cost, as it can be performed with disposable electrodes and a low-cost potentiostat. In summary, the association of E-t-i data with second-order calibration techniques represents an analytical strategy with outstanding features, as it allows electroactive species in complex samples to be determined without taking big precautions regarding interference minimization or removal (sample treatment, electrode modification, matrix matching etc.), significantly simplifying the analytical process.

5. ACKNOWLEDGEMENTS

The authors are grateful for the financial support of Coordenação de Aperfeiçoamento de Pessoal de Nível Superior – Brazil (CAPES) through the CAPES-PrInt Program, and Conselho Nacional de Desenvolvimento Científico e Tecnológico – Brazil (CNPq, grant number 313738/2018-1).

6. REFERENCES

[1]. Reilley, C. H.; Cooke, W. D.; Furman, N. H. *Anal. Chem*. **1951**, *23*, 1226-1229.

[2]. Reinmuth, W. H. *Anal. Chem*. **1960**, *32*, 1509-1512.

[3]. Anderson, J. E.; Bond, A. M. *J. Electroanal. Chem*. **1983**, *145*, 21-34.

[4]. Papadopoulos, N.; Hasiotis, C.; Kokkinidis, G.; Papanastasiou, G. *Electroanal*. **1993**, *5*, 99-102.

[5]. Bond, A. M.; Henderson, T. L. E.; Oldham, K. B. *J. Electroanal. Chem.* **1985**, *191*, 75-90.

[6]. Sun, S. G.; Lipkowski, J.; Altounian, Z. *J. Electrochem. Soc.* **1990**, *137*, 2443-2451.

[7]. Papadopoulos, N.; Hasiotis, C.; Kokkinidis, G.; Papanastasiou, G. *Electroanal. Chem*. **1991**, *308*, 83-96.

[8]. Torres, M.; Díaz-Cruz, J.M.; Ariño, C.; Grabaric, B. S.; Esteban, M. *Electroanal.* **1999**, *11*, 93-100.

[9]. Bond A. M., Heritage I. D.; Thormann W. *Anal. Chem.* **1986**, *58*, 1063-1066.

[10]. Bro, R. *Chemom. Intell. Lab. Syst.* **1997**, *38*, 149-171

[11]. Tauler, R. *Chemom. Intell. Lab. Syst.* **1995**, *30*, 133-146.

[12]. Ho, C. N.; Christian, G. D.; Davidson, E. R. *Anal. Chem.* **1978**, *50*, 1108.

[13]. Galeano-Dıaz, T.; Guiberteau-Cabanillas, A.; Espinosa-Mansilla, A.; Lopez-Soto, M. D. *Anal. Chim. Acta* **2008**, *618*, 131–139

[14]. Abdollahi, H.; Kooshki, M. *Electroanal.* **2010**, *22*, 2245–2253.

[15]. Kooshki, M.; Abdollahi, H.; Bozorgzadeh, S.; Haghighi, B. *Electrochim. Acta* **2011**, *56*, 8618–8624.

[16]. Jalalvand, A. R.; Gholivand, M.-B.; Goicoechea, H. C.; Skov, T. *Talanta* **2015**, *134*, 607–618.

[17]. Heydari, M.; Ghoreishi, S. M.; Khoobi, A. *Food Chem.* **2019**, *283*, 68–72.

[18]. Yazan, Z.; Erden, S.; Dinç, E. *J. Electroanal. Chem.* **2018**, *826*, 133–141

[19]. Silva, A. C.; Lourenço, A. S.; Araujo, M. C. U. *Food Chem.* **2018**, *266*, 232–239

[20]. Hemmateenejad, B.; Safavi, A.; Honarasa, F. *Anal. Methods* **2012**, *4*, 1776-1782

[21]. Bard, A. J.; Faulkner, L. R. *Electrochemical Methods: Fundamentals and Applications*, 2ed, Wiley, New York, **2001**.

[22]. Stojanovic, R. S.; Greenhill, H. B.; Bond, A. M.; Anderson, J. E. *Computers Chem.* **1996***, 20,* 209-218

[23]. Pitman, K.; Nerut, J.; Lust, E.; Franssila, S.; Raud, M.; Kikas, T.; *ECS Transactions* **2017**, *77*, 1771-1782

[24]. Rodrigues, D. R.; Olivieri, A. C.; Fragoso, W. D.; Lemos, S. G.; *Anal. Chim. Acta* **2019**, *1080*, 1-11.

[25]. Graham, G. G.; Scott, K. F.; Day, R. O. *Drug. Saf.* **2005**, *28*, 227

[26]. Modick, H.; Weiss, T.; Dierkes, G.; Brüning, T.; Koch, H. M.; *Reproduction* **2014**, *147*, 105-117

[27]. Raghavendran, H. R. B.; Sathivel, A.; Devaki, T. *J. Health Sci.* **2004**, *50*, 42.

[28]. Kang, M.; An, S. S. A. *Toxicol. Environ. Health. Sci.* **2010**, *2*, 278-283.

[29]. Taguchi, G.; Phadke, M.S. Quality Engineering through Design Optimization. In: Dehnad K. (eds) *Quality Control, Robust Design, and the Taguchi Method*. Springer, Boston, **1989**.

[30]. Smilde, A.; Bro, R.; Geladi, P. *Multi-Way Analysis with Applications in the Chemical Sciences*. John Wiley & Sons, **2004**

[31]. Olivieri, A. C.; Escandar, G. M.; de la Pena, A. M. *Trends Anal. Chem.* **2011**, *30*, 607-617

[32]. Marreto, P. D.; Zimer, A. M.; Faria, R. C.; Mascaro, L. H.; Pereira, E. C.; Fragoso, W. D.; Lemos, S. G. *Electrochim. Acta* **2014**, *127*, 68–78

[33]. Kooshki, M.; Díaz-Cruz, J. M.; Abdollahi, H.; Ariño, C.; Esteban, M. *Analyst* **2011**, *136*, 4696–4703.

[34]. Farahani, K. Z.; Benvidi, A.; Rezaeinasab, M.; Abbasi, S.; Abdollahi-Alibeik, M.; Rezaeipoor-Anari, A.; Zarchi, M. A. K.; Abadi, S. S. A. D. M. *Talanta* **2019**, *192*, 439-447

[35]. Skov, T.; van den Berg, F.; Tomasi, G.; Bro, R., *J. Chemom.* **2006**, *20*, 484–497.

[36]. Bro, R.; Kiers, H. A. L. *J. Chemom.* **2003**, *17*, 274–286.

[37]. Rinnan, Å., Riu, J., Bro, R., *J. Chemometrics* **2007**, *21*, 76-86.

[38]. Olivieri, A.C., Escandar, G.M., *Practical Three-Way Calibration*, Elsevier, **2014**.

[39]. Andersen, C. M.; Bro, R.; *J. Chemometrics* **2003**, *17*, 200–15.

[40]. Jaumot, J.; Gargallo, R.; Juan, A.; Tauler, R. *Chemom. Intell. Lab. Syst.* **2005**, *76*, 101–110.

[41]. Olivieri, A. C.; Wu, H. -L.; Yu, R. -Q. *Chemom. Intell. Lab. Syst.* **2009**, *96*, 246-251

[42]. Abreu, R. E. L.; Paz, J. E. M.; Silva, A. C.; Pontes, M. J. C.; Lemos, S. G. *Fuel* **2015**, *156*, 20–25

[43]. Rice, R. J.; Pontikos, N. M.; McCreery, R. L. *J. Am. Chem. Soc.* **1990**, *112*, 4617–4622

[44]. Chen, P.; McCreery, R. L. *Anal. Chem.* **1996**, *68*, 3958–3965

[45]. Shrestha, B. R.; Tada, T.; Nishikata, A.; *Electrochim. Acta* **2014**, *143*, 161-167

[46]. Geiger, S.; Cherevko, S.; Mayrhofer, K. J. J.; *Electrochim. Acta* **2015**, *179*, 24-31

[47]. Enache, T. A.; Oliveira-Brett, A. M. *J Electroanal Chem* **2011**, 655, 9-16

[48]. Filik, H.; Avan, A. A.; Aydar, S.; Çetintaş, G. *Int. J. Electrochem. Sci.* **2014**, *9*, 148 - 160

[49]. Bagheri, H.; Pajooheshpour, N.; Jamali, B.; Amidi, S.; Haji, A.; Khoshsafar, H. *Microchem. J.* **2017**, *131*, 120-129

[50]. Nematollahia, D.; Shayani-Jama, H.; Alimoradib, M.; Niroomand S. *Electrochim Acta* **2009**, *54*, 7407–7415